Journal of Computational Physics 228 (2009) 4162–4181

Contents lists available at ScienceDirect

Journal of Computational Physics

journal homepage: www.elsevier.com/locate/jcp

A phase field method for simulating morphological evolution of vesicles in electric fields

Ling-Tian Gao [a], Xi-Qiao Feng [a,*], Huajian Gao [b]

[a] Institute of Biomechanics and Medical Engineering, FML, Department of Engineering Mechanics, Tsinghua University, Beijing 100084, China
[b] Division of Engineering, Brown University, Providence, RI 02912, USA

ARTICLE INFO

Article history:
Received 5 June 2008
Received in revised form 17 February 2009
Accepted 20 February 2009
Available online 6 March 2009

PACS:
77.84.Nh
87.10.Kn

Keywords:
Phase field method
Mechanical–electrical coupling
Flexoelectricity
Biological interfaces
Cell membrane
Electric effects

ABSTRACT

A phase field method is developed to investigate the morphological evolution of a vesicle in an electric field, taking into account coupled mechanical and electric effects such as bending, osmotic pressure, surface tension, flexoelectricity, and dielectricity of the membrane. The energy of the system is formulated in terms of a continuous phase field variable and the electric potential. The governing equations of the phase field and the electric field are solved using the Galerkin weighted residual approach. The validation and robustness of the algorithm are verified by direct comparisons of the obtained numerical solutions with relevant experimental results. The morphological evolution of an axisymmetric vesicle under an electric field is studied in detail. The results demonstrate that the present method can simulate complex morphological evolutions of vesicles under coupled mechanical–electrical fields.

1. Introduction

Cell membrane plays a crucial role in many biological processes owing to their unique physical properties [1,2]. Cells can sense their environment and respond to external stimuli [3,4]. Such biological processes as growth, hybridization, migration, proliferation and differentiation of cells are closely related to the electrophysiological properties of cell membrane [3]. Various phenomena including electroporation, electrofusion, electrophoresis, and electro-deformation have been widely utilized in biophysical, biochemical and biomechanical studies of cells such as transfer/delivery of genes, proteins, antibodies or drugs into cells, separation of different kinds of biological macromolecules or cells, and measurement of different physical properties of the cell membrane [1,5–12].

In the past several years, considerable effort has been directed towards understanding and predicting the complicated morphological evolution of vesicles in an electric environment [13–19]. For example, Riske and Dimova [16] predicted a prolate-to-oblate transition in an electric field, depending on the ratio between the conductivity coefficients of the inner and outer electrolytes. Besides the electrical field, various effects from the fluid environment around the vesicle, such as the osmotic pressure, surface tension [1,20,21] and shear flow [22–28], also significantly influence the static and dynamic

* Corresponding author. Tel.: +86 10 6277 2934; fax: +86 10 6278 1824.
E-mail address: fengxq@tsinghua.edu.cn (X.-Q. Feng).

0021-9991/$ - see front matter © 2009 Elsevier Inc. All rights reserved.
doi:10.1016/j.jcp.2009.02.034

behaviors of the vesicle. Due to the intrinsic complexity of mechanical–electrical coupling and nonlinear geometric deformation of cells, existing theoretical studies have been largely confined to relatively simple configurations (e.g., infinite planes, spheres and ellipses). Recently, Gao et al. [19] developed a more general liquid crystal model for vesicles subjected to arbitrary electric fields, taking into account such effects as elastic bending, osmotic pressure, surface tension, flexoelectricity, dielectricity, and Maxwell electric pressure of the membrane.

Various numerical methods have been developed to investigate vesicle behaviors under mechanical loading, e.g., finite difference method [20] and finite element method [29–31]. In the presence of an electric field, the behavior of vesicles can become significantly more complicated. Accounting for the Maxwell pressure on the inner and outer sides of the membrane, Hyuga et al. [32,33] developed a semi-analytical perturbation method to calculate the static and dynamic deformation of conductive vesicles. However, this method seems to be limited to problems with weak nonlinearity. A boundary integral approach was adopted by Fan and Fedorov [34] to study the interaction between an AFM tip and a biomembrane in a dilute electrolyte solution. However, this type of methods does not allow for a large topological change and their applications are limited to situations where the governing equations in the bulk phase are linear [35]. The level set method [36,37] and arbitrary Lagrange–Euler method (ALE) [38], which have been widely used in simulations of multiphase flows, dynamic bubbles and drops, can also be used to simulate the morphological evolution of vesicles. However, the level set method often faces difficulties in the renormalization procedure, while the mesh mapping, configuration changing and refinement procedure in the ALE strategy can compromise efficiency and accuracy, especially for strongly nonlinear problems like those studied in the present paper.

The phase field method has provided a powerful tool to solve moving boundary problems involving coupled physical fields (e.g., electric, magnetic, fluidic, and chemical fields). This method is based on a phase field which is assumed to be continuous over boundaries and has the physical meaning of an order parameter. The energy of the system is expressed in terms of the phase field variable, and the morphological evolution can be described without explicitly tracking the boundary. The phase field method has some advantages in dealing with moving boundaries, large deformation, morphological singularity and energy dissipation, and it can be used to simulate complicated microstructure evolution (e.g., solidification, phase transformation, grain growth and domain evolution in thin films) [39]. Recently, Biben and Misbah [40] proposed a phase field model to investigate the tumbling of vesicles under shear flow, and they also extended this approach to three-dimensional vesicle dynamics [35]. Du et al. [41] developed a phase field method to systematically analyze the morphological evolution of vesicles. A similar procedure was developed by Campelo and Hernandez-Machado [42] to simulate the dynamic and stationary shapes of vesicles. Du et al. [41] and Campelo and Hernandez-Machado [42] made use of finite difference and spectrum discretization algorithms, respectively. More recently, Du et al. developed a mixed finite element method to study the equilibrium configuration of vesicle membrane [43] and the dynamics of vesicle membranes in incompressible viscous fluids [44]. They also developed an adaptive FEM approach [45] for handling complex shape and topological changes. However, the electric effects have not been addressed in the previously studies.

In this paper, a phase field model, based on the liquid crystal model of Gao et al. [19], is developed to investigate the morphological evolution of vesicles under arbitrary mechanical and electric fields. We will use the finite element method to discretize the phase field variable, which has certain advantages in treating inhomogeneous material properties as well as complex material interfaces and topology. We will examine in some detail the effects of mechanical–electric coupling, inner and outer electrolytes, flexoelectricity and dielectricity on the morphological evolution of a vesicle and compare the numerical results to relevant experiments.

2. Liquid crystal model of vesicles under mechanical and electric fields

Experimental observations have demonstrated that cell membranes are constructed based on the general principles of liquid crystal lipid bilayers [9,46]. The elastic theory of liquid crystal biomembranes has been successfully applied to study the morphological change, adhesion, and some other related problems of cell membranes [47–50]. However, there is surprisingly little investigation on the effect of flexoelectricity on the behavior of cell membranes. When subjected to strong electric pulses, some unusual deformations of vesicles changing among disc-, square-, and tube-like shapes have been experimentally observed. These phenomena cannot be explained by a liquid crystal model that disregards the electric conductivity of the cell membrane and the electrolyte. In response to recent advances in experimental observations, we proposed a more general electromechanical liquid crystal model of cell membranes based on Eringen's micropolar theory [51]. The model accounts for contributions of elastic bending, osmotic pressure, surface tension, flexoelectric and dielectric effects under various types of mechanical and electrical fields.

In this section, the liquid crystal model of vesicles under mechanical and electric fields [19] is briefly reviewed.

Consider a quasi-static configuration of a dielectric lipid vesicle in an electric field, the Helmholtz free energy of the system can be expressed as

$$F = F_{\mathrm{bm}} + F_{\mathrm{fm}} + F_{\mathrm{dm}} + F_{\mathrm{de}}, \tag{1}$$

where $F_{\mathrm{bm}}, F_{\mathrm{fm}}$, and F_{dm} are the elastic bending energy, the flexoelectric energy, and the dielectric energy of the membrane, respectively, and F_{de} is the dielectric energy of the electrolyte.

According to Helfrich [52], the elastic bending energy is given by

$$F_{\mathrm{bm}} = \int_{\Gamma} \left[\frac{1}{2} k (2H + c_0)^2 + k_{\mathrm{k}} K \right] \mathrm{d}A, \tag{2}$$

where Γ denotes the surface of the vesicle, k and k_{k} are elastic constants, H is the mean curvature, K is the Gauss curvature, and c_0 is the spontaneous curvature.

The flexoelectric energy F_{fm} associated with the electroelastic coupling effects of the membrane is written as [21]

$$F_{\mathrm{fm}} = -\int_{\Gamma} \int_0^d \mathbf{P}^{\mathrm{fm}} \cdot \mathbf{E} \, \mathrm{d}r \, \mathrm{d}A, \tag{3}$$

where d is the thickness of the membrane and $\mathbf{E}$ is the electric field intensity. The polarization $\mathbf{P}^{\mathrm{fm}}$ caused by bending is given as

$$\mathbf{P}^{\mathrm{fm}} = -e_{11} (\nabla \cdot \mathbf{n}) \mathbf{n}, \tag{4}$$

where e_{11} is the flexoelectric coefficient and $\mathbf{n}$ is the unit normal vector of the membrane surface.

The dielectric energy is expressed as

$$F_{\mathrm{dm}} = -\frac{1}{2} \int_{\Gamma} \int_0^d \mathbf{D}^{\mathrm{em}} \cdot \mathbf{E} \, \mathrm{d}r \, \mathrm{d}A, \tag{5}$$

where the electric displacement $\mathbf{D}^{\mathrm{em}}$ can be decomposed as

$$\mathbf{D}^{\mathrm{em}} = (\varepsilon_{\perp} + \varepsilon_{\parallel}) E_{\mathrm{n}} \mathbf{n} + \varepsilon_{\perp} E_u \mathbf{Y}_{,u} + \varepsilon_{\perp} E_v \mathbf{Y}_{,v}, \tag{6}$$

$\varepsilon_{\parallel}$ and $\varepsilon_{\perp}$ denoting the anisotropic dielectric constants along and normal to the $\mathbf{n}$ direction [53], respectively. The parameterized function $\mathbf{Y} = \mathbf{Y}(u, v)$ describes the membrane surface in terms of two variables u and v, as shown in Fig. 1, which can take different forms in different coordinates. The surface parameters u and v are properly defined such that the axes along $\mathbf{Y}_{,u}$ and $\mathbf{Y}_{,v}$ are orthogonal; E_u and E_v are the magnitudes of the electric field in the $\mathbf{Y}_{,u}$ and $\mathbf{Y}_{,v}$ directions, respectively. We further define $g_{uu} = \mathbf{Y}_{,u} \cdot \mathbf{Y}_{,u}$ and $g_{vv} = \mathbf{Y}_{,v} \cdot \mathbf{Y}_{,v}$ to be used in the following formulations. The normal vector $\mathbf{n}$ and the two tangential vectors $\mathbf{Y}_{,u}$ and $\mathbf{Y}_{,v}$ constitute a local orthogonal coordinate system.

The dielectric energy of an electrolyte is expressed as

$$F_{\mathrm{de}} = -\int_{\Omega} \frac{1}{2} \varepsilon_{\mathrm{r}} |\nabla \phi|^2 \, \mathrm{d}V, \tag{7}$$

where ε_{r} denotes the dielectric constant of the electrolyte and ϕ the electric potential.

We define the following energy functional [19]

$$F_0 = F_{\mathrm{bm}} + F_{\mathrm{fm}} + F_{\mathrm{dm}} + F_{\mathrm{de}} + \Delta p (V - V_0) + \gamma (A - A_0), \tag{8}$$

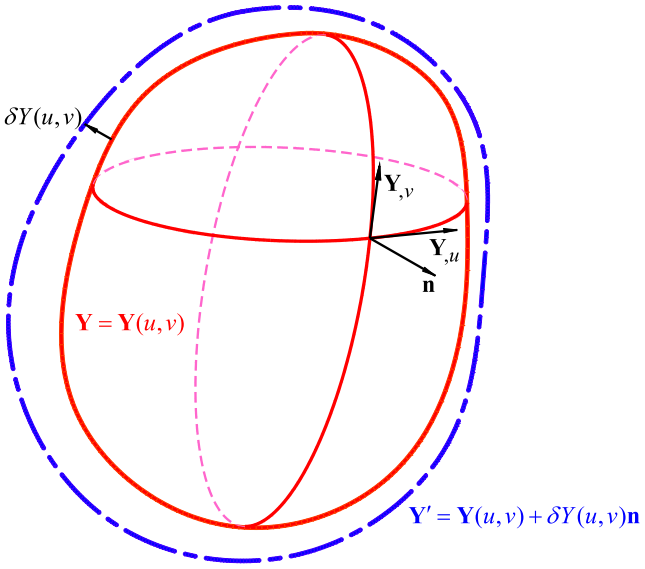

Fig. 1. Schematic of a vesicle described by a parameterized shape function $\mathbf{Y} = \mathbf{Y}(u, v)$ with a local orthogonal coordinate system $(\mathbf{Y}_{,u}, \mathbf{Y}_{,v}, \mathbf{n})$ and a small normal variation $\delta Y(u, v)\mathbf{n}$.

where $\Delta p = p_{out} - p_{in}$ is the osmotic pressure, γ is the surface tension of the membrane, V_0 and A_0 denote the initial volume and surface area of the vesicle before loading, and V and A denote the volume and surface area of the deformed vesicle under loading, respectively. p_{in} and p_{out} are the pressure in and out of the vesicle, respectively. Both Δp and γ, which are also referred to as Lagrange multipliers from the viewpoint of mathematics [21], are assumed to remain constant during the deformation of the vesicle. The associated constraint equations will be discussed in Section 3. The last two terms in Eq. (8) stand for the work done by the osmotic pressure and by the surface tension due to changes of the vesicle volume and surface area, respectively.

From the first-variational condition $\delta F = 0$, the Euler–Lagrange equation of shape evolution for a vesicle under mechanical and electric fields is derived as [19]

$$\begin{cases} \nabla^2\left(2kH + kc_0 - e_{11}\int_0^d E_n \,\mathrm{d}r\right) + f = 0, \\ f = k(2H + c_0)(2H^2 - c_0H - 2K) + \Delta p - 2\gamma H \\ \quad +H\int_0^d[(\varepsilon_\perp + \varepsilon_\parallel)E_n^2 + \varepsilon_\perp g_{uu}E_u^2 + \varepsilon_\perp g_{vv}E_v^2]\,\mathrm{d}r \\ \quad +2e_{11}K\int_0^d E_n\,\mathrm{d}r + \varepsilon_i(E_{in}^2 - 1/2\mathbf{E}_i^2) - \varepsilon_o(E_{on}^2 - 1/2\mathbf{E}_o^2). \end{cases} \tag{9}$$

This equation has accounted for coupling between electric and mechanical energy terms, and it will be used to investigate the behavior of a vesicle under electric fields.

For a static electric field, one has

$$\nabla\cdot(\sigma\nabla\phi) = 0, \tag{10}$$

where the conductivity σ takes the value $\sigma = \sigma_o$ in the outer electrolyte, $\sigma = \sigma_i$ in the inner electrolyte, and $\sigma = \sigma_m$ in the membrane. The electric boundary conditions are

$$\begin{cases} \phi_m = \phi_o, & \sigma_m\frac{\partial\phi_m}{\partial n} = \sigma_o\frac{\partial\phi_o}{\partial n}, \quad \text{on } \Gamma_{om}, \\ \phi_m = \phi_i, & \sigma_m\frac{\partial\phi_m}{\partial n} = \sigma_i\frac{\partial\phi_i}{\partial n}, \quad \text{on } \Gamma_{im}, \\ \phi_o|_{r\to\infty} = -E_0 z, \\ \phi_o|_{r\to 0} = 0, \end{cases} \tag{11}$$

where Γ_{om} and Γ_{im} denote the outer and the inner boundaries of the membrane, respectively.

In principle, the morphology of a vesicle under an electric field can be determined by simultaneously solving the shape equation (9) and the electric field equation (10), in conjunction with the boundary conditions in (11). This problem is highly nonlinear and has moving boundaries. In the next section, we will construct an efficient phase field method to solve these equations.

3. Phase field formulation

3.1. Phase field variable

Following Du et al. [41], we adopt the following phase function

$$C(\mathbf{x}) = f\left[\frac{di(\mathbf{x})}{\sqrt{2}b}\right] = \tanh\left[\frac{di(\mathbf{x})}{\sqrt{2}b}\right], \tag{12}$$

where b denotes the thickness of an interface. The parameter b equals to zero for a theoretically sharp interface, but is generally taken to be a small value in numerical simulations. The function $di(\mathbf{x})$ is a signed distance function [36] satisfying $di(\mathbf{x}) = 0$ for $\mathbf{x}\in\Gamma$ on the boundary Γ; $di(\mathbf{x}) < 0$ for $\mathbf{x}\in\Omega$ inside the domain Ω; and $di(\mathbf{x}) > 0$ for $\mathbf{x}\notin(\Omega\cup\Gamma)$ outside the domain Ω. It is also noted that $\nabla di(\mathbf{x}) = \mathbf{n}$, where $\mathbf{n}$ is the outward unit vector normal to the interface Γ.

From the relations $f' = 1 - f^2, f'' = -2f(1-f^2)$ and $\nabla C(\mathbf{x}) = f'\frac{\nabla di(\mathbf{x})}{\sqrt{2}b}$, the unit vector $\mathbf{n}$ is expressed as

$$\mathbf{n} = \nabla di(\mathbf{x}) = \frac{\sqrt{2}b}{f'}\nabla C = \frac{\sqrt{2}b}{1-C^2}\nabla C. \tag{13}$$

From $\nabla^2 C(\mathbf{x}) = f''\frac{[\nabla di(\mathbf{x})]^2}{2b^2} + f'\frac{\nabla^2 di(\mathbf{x})}{\sqrt{2}b}$ and $[\nabla di(\mathbf{x})]^2 = \mathbf{n}\cdot\mathbf{n} = 1$, one has

$$\nabla\cdot\mathbf{n} = \nabla^2 di(\mathbf{x}) = \frac{\sqrt{2}b}{f'}\left(\nabla^2 C - \frac{f'}{2b^2}\right) = \frac{\sqrt{2}b}{(1-C^2)}\left[\nabla^2 C + \frac{1}{b^2}C(1-C^2)\right]. \tag{14}$$

The mean curvature H is expressed in terms of the phase field variable C as

$$H = -\frac{1}{2}\nabla^2 di(\mathbf{x}) = -\frac{\sqrt{2}b}{2(1-C^2)}\left[\nabla^2 C + \frac{1}{b^2}C(1-C^2)\right]. \tag{15}$$

3.2. Free energy and shape equation in terms of the phase field variable

The phase equation $f(x)$ in Eq. (12) satisfies the following relations [54]:

$$f'(x) = 1 - \tanh^2(x) = \operatorname{sech}^2(x), \tag{16}$$

$$\int_{-\infty}^{+\infty} \left[1 - f^2\left(\frac{\tau}{\sqrt{2}b}\right)\right]^2 \mathrm{d}\tau = \int_{-\infty}^{+\infty} \operatorname{sech}^4\left(\frac{\tau}{\sqrt{2}b}\right)\mathrm{d}\tau = \frac{4\sqrt{2}b}{3} \quad \text{for } b > 0, \tag{17}$$

$$\lim_{\tau\to\infty} f\left(\frac{\tau}{\sqrt{2}b}\right)\tau = \lim_{\tau\to\infty} \operatorname{sech}^4\left(\frac{\tau}{\sqrt{2}b}\right)\tau = 0. \tag{18}$$

Using Eqs. (12), (13), (15) and (17) and considering the small membrane thickness d as a constant, the energies in Eqs. (2), (3), (5) and (7) will be reformulated in terms of the phase field variable C.

First, the bending energy $\overline{F}_{\mathrm{bm}}$ in Eq. (2) becomes

$$\overline{F}_{\mathrm{bm}} = \int_\Gamma \frac{k}{2}(2H + c_0)^2\,\mathrm{d}A \approx \frac{3k}{4\sqrt{2}b}\int_{\Omega_1}\left[b\nabla^2 C + \left(\frac{1}{b}C - \frac{\sqrt{2}}{2}c_0\right)(1 - C^2)\right]^2 \mathrm{d}V, \tag{19}$$

where Ω_1 includes the membrane and the electrolyte domain. Using the relation $\mathbf{E} = -\nabla\phi$, the flexoelectric energy in Eq. (3) can be re-expressed as

$$\overline{F}_{\mathrm{fm}} = -2e_{11}\int_\Gamma H\int_0^d E_{\mathrm{n}}\,\mathrm{d}r\,\mathrm{d}A = -2e_{11}d\int_\Gamma H\mathbf{E}\cdot\mathbf{n}\,\mathrm{d}A \approx -\frac{3e_{11}d}{2\sqrt{2}}\int_{\Omega_1}\left[b\nabla^2 C + \frac{1}{b}C(1 - C^2)\right](\nabla\phi)(\nabla C)\,\mathrm{d}V. \tag{20}$$

Similarly, the dielectric energy of the membrane in Eq. (5) can be rewritten as

$$\overline{F}_{\mathrm{dm}} = -\int_\Gamma \frac{1}{2}\varepsilon_{\mathrm{m}}\int_0^d |\nabla\phi|^2\,\mathrm{d}r\,\mathrm{d}A = -\int_\Gamma \frac{1}{2}\varepsilon_{\mathrm{m}}d|\nabla\phi|^2\,\mathrm{d}A \approx -\frac{3d}{8\sqrt{2}b}\int_{\Omega_1}\varepsilon_{\mathrm{m}}(1 - C^2)^2|\nabla\phi|^2\,\mathrm{d}V. \tag{21}$$

From Eq. (13) and using the relation $\mathbf{n}\cdot\mathbf{n} = 1$, we have

$$(1 - C^2)^2 = 2b^2|\nabla C|^2. \tag{22}$$

Then the dielectric energy in Eq. (21) becomes

$$\overline{F}_{\mathrm{dm}} \approx -\frac{3db}{4\sqrt{2}}\int_{\Omega_1}\varepsilon_{\mathrm{m}}|\nabla C|^2|\nabla\phi|^2\,\mathrm{d}V. \tag{23}$$

The dielectric energy of the electrolyte in Eq. (7) is reformulated in terms of the phase variable C as

$$\overline{F}_{\mathrm{de}} = -\int_{\Omega_1}\frac{1}{2}\varepsilon_{\mathrm{r}}(C)|\nabla\phi|^2\,\mathrm{d}V, \tag{24}$$

where $\varepsilon_{\mathrm{r}}(C) = \frac{1}{2}\varepsilon_{\mathrm{i}}(1 - C) + \frac{1}{2}\varepsilon_{\mathrm{o}}(1 + C)$.

Using the phase field variable, the vesicle volume and the interface area of the deformed vesicle are expressed as

$$\overline{V} = \frac{1}{2}\int_{\Omega_1}(1 - C)\,\mathrm{d}V, \tag{25}$$

$$\overline{A} = \int_\Gamma \mathrm{d}A \approx \frac{3}{4\sqrt{2}b}\int_{\Omega_1}(1 - C^2)^2\,\mathrm{d}V = \frac{3b}{2\sqrt{2}}\int_{\Omega_1}|\nabla C|^2\,\mathrm{d}V. \tag{26}$$

Finally, the energy functional in Eq. (8) is recast as

$$\overline{F} = \overline{F}_{\mathrm{bm}} + \overline{F}_{\mathrm{fm}} + \overline{F}_{\mathrm{dm}} + \overline{F}_{\mathrm{de}} + \Delta p\int_{\Omega_1} L_1\,\mathrm{d}V + \gamma\int_{\Omega_1} L_2\,\mathrm{d}V, \tag{27}$$

where

$$L_1 = \frac{1}{2}(1 - C) - \frac{V_0}{V_1}, \quad L_2 = \frac{3b}{2\sqrt{2}}|\nabla C|^2 - \frac{A_0}{V_1}, \tag{28}$$

$V_1 = \int_\Omega \mathrm{d}V$ being the total volume of the calculation domain. The shape equation is determined by minimizing $\overline{F}$ with respect to C, i.e.,

$$\frac{\delta\overline{F}(C)}{\delta C} = 0. \tag{29}$$

The steepest decent approach [55] is adopted to solve the phase field equation (29):

$$\frac{\partial C}{\partial t} = -\frac{\delta \overline{F}(C)}{\delta C}, \tag{30}$$

where

$$\frac{\delta \overline{F}(C)}{\delta C} = \frac{\partial \overline{F}}{\partial C} - \nabla \cdot \frac{\partial \overline{F}}{\partial (\nabla C)} + \nabla^2 \frac{\partial \overline{F}}{\partial (\nabla^2 C)}. \tag{31}$$

Finally, the phase field equation for the morphology of vesicle in an electric field is derived as

$$\begin{cases} \frac{\partial C}{\partial t} + \nabla^2 P - \nabla \cdot \mathbf{F}_2 + F_1 = 0, \\ P = \alpha_3 \nabla^2 C + \boldsymbol{\beta}_3 \cdot \nabla C + \gamma_3, \end{cases} \tag{32}$$

where

$$\begin{aligned} F_1 &= \frac{\partial \overline{F}}{\partial C} = \frac{P}{b^2}(1 - 3C^2 + C\sqrt{2}c_0 b) + \frac{3}{2}e_{11}d_0 c_0 C(\nabla C \cdot \nabla \phi) - \frac{\Delta p}{2} + \frac{1}{4}(\varepsilon_i - \varepsilon_o)(\nabla \phi)^2, \\ \mathbf{F}_2 &= \frac{\partial \overline{F}}{\partial (\nabla C)} \\ &= -\frac{e_{11}d_0}{k} P \nabla \phi + \frac{3}{4}e_{11}d_0 c_0 (C^2 - 1)\nabla \phi \\ &\quad + \left[\frac{3\sqrt{2}}{2} b\gamma - \frac{3\sqrt{2}d_0 b}{4k}(e_{11}^2 d_0 + \varepsilon_m k)(\nabla \phi)^2\right] \nabla C, \\ \alpha_3 &= \frac{3\sqrt{2}}{4} kb, \quad \boldsymbol{\beta}_3 = -\frac{3\sqrt{2}}{4} e_{11} d_0 b \nabla \phi, \\ \gamma_3 &= \frac{3\sqrt{2}k}{8b}(-2C + \sqrt{2}c_0 b)(-1 + C^2). \end{aligned} \tag{33}$$

3.3. Constraint conditions

The two equations in (32) contain five independent variables, namely, the phase field variable C, the intermediate variable P, the electric potential ϕ, and the osmotic pressure Δp and the surface tension γ. Therefore, three more constraint equations are needed, which are given from the governing equation of the electric field and the constraint conditions of the volume and area of the vesicle. In the present paper, we assume that the surface area of the vesicle does not change during deformation, but its volume may vary.

The first complementary equation is the steady electric field equation (10), which is recast in terms of the phase field variable C as

$$\nabla \cdot (\sigma_r \nabla \phi) = 0, \tag{34}$$

where

$$\sigma_r(C) = \frac{1}{2}\sigma_i(1 + C) + \sigma_m(1 + C)(1 - C) + \frac{1}{2}\sigma_o(1 - C). \tag{35}$$

Since the conductivity of the vesicle σ_m is generally much smaller than those of the electrolytes σ_o and σ_i, there exist discontinuities or steep jumps of the conductivity coefficients across the inner and outer interfaces. Eq. (35) cannot well describe the variation of the conductivity across the membrane–electrolyte interfaces. In our simulations, Eq. (35) is replaced by the following modified interpolation function

$$\sigma = \frac{\sigma_i}{4}(1 - C)^2 C^8 + \frac{\sigma_m}{4}(1 - C)^2(1 + C)^2 + \frac{\sigma_o}{4}(1 + C)^2 C^8. \tag{36}$$

The multiplier penalty method [56] is adopted to introduce the constraint conditions of the volume and surface area of the deformed vesicle. Thereby, we define a modified energy functional by adding a power penalty term with a parameter c_1 into Eq. (27):

$$\overline{F}_1 = \overline{F}_{bm} + \overline{F}_{fm} + \overline{F}_{dm} + \overline{F}_{de} + \Delta p \int_{\Omega_1} L_1 \, dV + \gamma \int_{\Omega_1} L_2 \, dV + \frac{c_1}{2} \int_{\Omega_1} L_1^2 \, dV. \tag{37}$$

Minimization of $\overline{F}_1$ with respect to the phase field variable C yields the first complementary equation

$$\Delta p A_1 + \gamma B_1 + C_1 + c_1 D_1 = 0, \tag{38}$$

where A_1, B_1, C_1, and D_1 are given as

$$\begin{aligned}
A_1 &= \int_{\Omega_1} \frac{\delta L_1}{\delta C}\,\mathrm{d}V = -\frac{1}{2}\int_{\Omega_1}\mathrm{d}V,\\
B_1 &= \int_{\Omega_1} \frac{\delta L_2}{\delta C}\,\mathrm{d}V = -\frac{3\sqrt{2}b}{2}\int_{\Omega_1}\nabla^2 C\,\mathrm{d}V,\\
C_1 &= \int_{\Omega_1} \frac{\delta(\overline{F}_{\mathrm{bm}}+\overline{F}_{\mathrm{fm}}+\overline{F}_{\mathrm{dm}}+\overline{F}_{\mathrm{de}})}{\delta C}\,\mathrm{d}V = \int_{\Omega_1}(\nabla^2 P - \nabla\cdot\widetilde{\mathbf{F}}_2 + \widetilde{F}_1)\,\mathrm{d}V,\\
D_1 &= \frac{1}{2}\int_{\Omega_1}\frac{\delta L_1^2}{\delta C}\,\mathrm{d}V = \frac{1}{2}\int_{\Omega_1}\left(\frac{C-1}{2}+\frac{V_0}{V_1}\right)\mathrm{d}V,
\end{aligned} \tag{39}$$

with

$$\begin{aligned}
\widetilde{\mathbf{F}}_2 &= -\frac{e_{11}d_0}{k}P\nabla\phi + \frac{3}{4}e_{11}d_0c_0(C^2-1)\nabla\phi\\
&\quad -\frac{3\sqrt{2}d_0b}{4k}(e_{11}^2 d_0+\varepsilon_{\mathrm{m}}k)(\nabla\phi)^2\nabla C,\\
\widetilde{F}_1 &= \frac{P}{b^2}(1-3C^2+C\sqrt{2}c_0b)\\
&\quad +\frac{3}{2}e_{11}d_0c_0C(\nabla C\cdot\nabla\phi)+\frac{1}{4}(\varepsilon_{\mathrm{i}}-\varepsilon_{\mathrm{o}})(\nabla\phi)^2.
\end{aligned}$$

Furthermore, the constant surface area of the vesicle requires

$$\int_{\Omega_1}\frac{\mathrm{d}L_2}{\mathrm{d}t}\,\mathrm{d}V = \int_{\Omega_1}\frac{\delta L_2}{\delta C}\frac{\partial C}{\partial t}\,\mathrm{d}V = 0. \tag{40}$$

Another functional is chosen as

$$\overline{F}_2 = \overline{F}_{\mathrm{bm}}+\overline{F}_{\mathrm{fm}}+\overline{F}_{\mathrm{dm}}+\overline{F}_{\mathrm{de}}+\Delta p\int_{\Omega_1}L_1\,\mathrm{d}V+\gamma\int_{\Omega_1}L_2\mathrm{d}V+\frac{c_2}{2}\int_{\Omega_1}L_2^2\,\mathrm{d}V, \tag{41}$$

where c_2 is a penalty parameter for constraining the surface area of the vesicle. By the standard gradient flow approach, we have

$$\frac{\partial C}{\partial t} = -\frac{\delta\overline{F}_2}{\delta C}. \tag{42}$$

Substitution of Eq. (42) into (40) leads to the second complementary equation

$$\int_{\Omega_1}\frac{\delta L_2}{\delta C}\frac{\delta F_2}{\delta C}\,\mathrm{d}V = \Delta pA_2+\gamma B_2+C_2+c_2D_2 = 0, \tag{43}$$

where A_2, B_2, C_2, and D_2 are given as

$$\begin{aligned}
A_2 &= \int_{\Omega_1}\frac{\delta L_2}{\delta C}\frac{\delta L_1}{\delta C}\,\mathrm{d}V = \frac{3\sqrt{2}b}{4}\int_{\Omega_1}\nabla^2 C\,\mathrm{d}V,\\
B_2 &= \int_{\Omega_1}\left(\frac{\delta L_2}{\delta C}\right)^2\mathrm{d}V = \frac{9}{2}b^2\int_{\Omega_1}(\nabla^2 C)^2\,\mathrm{d}V,\\
C_2 &= \int_{\Omega_1}\frac{\delta L_2}{\delta C}\frac{\delta(F'_{\mathrm{bm}}+F'_{\mathrm{fm}}+F'_{\mathrm{dm}}+F'_{\mathrm{de}})}{\delta C}\mathrm{d}V\\
&= -\frac{3\sqrt{2}b}{2}\int_{\Omega_1}(\nabla^2 P-\nabla\cdot\widetilde{\mathbf{F}}_2+\widetilde{F}_1)\nabla^2 C\,\mathrm{d}V,\\
D_2 &= \frac{1}{2}\int_{\Omega_1}\frac{\delta}{L_2}\delta C\frac{\delta^2}{L_2}\delta C\,\mathrm{d}V\\
&= \frac{9\sqrt{2}b^2}{8}\int_{\Omega_1}\left[9b(\nabla C)^2-\frac{2\sqrt{2}A_0}{V_1}\right]\left(\frac{C-1}{2}+\frac{V_0}{V_1}\right)(\nabla^2 C)^2\,\mathrm{d}V.
\end{aligned} \tag{44}$$

Eqs. (32), (34), (38) and (43) provide all the equations of the phase field approach for simulating the shape evolution of vesicles under mechanical and electric fields.

4. Finite element discretization of the phase field formulation

Now the strong formulation of the phase field Eqs. (32) and (34) is transformed into a weak form for the convenience of finite element discretization. Using the Galerkin weighted residual approach [57], the weak forms of these equations are

$$\begin{aligned}
&\int_{\Omega_1} [-\nabla C \cdot \nabla P_{\text{test}} + (\boldsymbol{\beta}_3 \cdot \nabla C + \gamma_3 - P) P_{\text{test}}/\alpha_3]\, \mathrm{d}V = 0,\\
&\int_{\Omega_1} \frac{\partial C}{\partial t} C_{\text{test}}\, \mathrm{d}V + \int_{\Omega_1} [-(\nabla P)\cdot(\nabla C_{\text{test}}) + \mathbf{F}_2 \cdot \nabla C_{\text{test}} + F_1 C_{\text{test}}]\, \mathrm{d}V = 0,\\
&\int_{\Omega_1} \sigma_{\text{r}}(\nabla\phi)\cdot(\nabla\phi_{\text{test}})\, \mathrm{d}V = 0,
\end{aligned} \tag{45}$$

where $C_{\text{test}}, P_{\text{test}}$, and ϕ_{test} are the test functions of the variable C, P, and ϕ, respectively. Their discretized forms are

$$\begin{aligned}
&C = \mathbf{N}^{\text{T}}\mathbf{C}, \quad C_{\text{test}} = \mathbf{N}^{\text{T}}\mathbf{C}^*,\\
&P = \mathbf{N}^{\text{T}}\mathbf{P}, \quad P_{\text{test}} = \mathbf{N}^{\text{T}}\mathbf{P}^*,\\
&\phi = \mathbf{N}^{\text{T}}\boldsymbol{\varphi}, \quad \phi_{\text{test}} = \mathbf{N}^{\text{T}}\boldsymbol{\varphi}^*,
\end{aligned} \tag{46}$$

where $\mathbf{N}$ is the shape function. The matrixes $\mathbf{C}, \mathbf{P}$, and $\boldsymbol{\varphi}$ denote the generalized displacements of the variables C, P, and ϕ; and $\mathbf{C}^*, \mathbf{P}^*$, and $\boldsymbol{\varphi}^*$ denote the generalized displacements of the test functions $C_{\text{test}}, P_{\text{test}}$, and ϕ_{test}, respectively. Using the second-order Lagrange element discretization in space and taking the variation with respect to $\mathbf{C}^*, \mathbf{P}^*$ and $\boldsymbol{\varphi}^*$, Eq. (45) is derived as

$$\begin{aligned}
&\mathbf{K}_{\text{a}}\mathbf{C} + \mathbf{K}_{\text{b}}(\boldsymbol{\varphi})\mathbf{C} + \mathbf{K}_{\text{c}}(\mathbf{C}) + \mathbf{K}_{\text{d}}\mathbf{P} = \mathbf{0},\\
&\mathbf{K}_{\text{a}}\mathbf{P} + \mathbf{K}_{\text{e}}(\mathbf{C}, \boldsymbol{\varphi}) + \mathbf{M}\frac{\partial \mathbf{C}}{\partial t} = \mathbf{0},\\
&\mathbf{K}_{\text{f}}(\mathbf{C})\boldsymbol{\varphi} = \mathbf{0},
\end{aligned} \tag{47}$$

where the coefficient matrixes are

$$\begin{aligned}
&K_{\text{a}ij} = -\int_{\Omega_1} (\nabla N_i)^{\text{T}} \nabla N_j\, \mathrm{d}V,\\
&K_{\text{b}ij}(\boldsymbol{\varphi}) = \frac{1}{\alpha_3}\int_{\Omega_1} (\nabla N_i)^{\text{T}} \boldsymbol{\beta}_3(\boldsymbol{\varphi}) N_j\, \mathrm{d}V,\\
&K_{\text{c}ij}(\mathbf{C}) = \frac{1}{\alpha_3}\int_{\Omega_1} N_i [\gamma_3(\mathbf{C})]_j\, \mathrm{d}V,\\
&K_{\text{d}ij} = -\frac{1}{\alpha_3}\int_{\Omega_1} N_i N_j\, \mathrm{d}V,\\
&K_{\text{e}ij}(\mathbf{C}, \boldsymbol{\varphi}) = \int_{\Omega_1} (\nabla N_i)^{\text{T}} [\mathbf{F}_2(\mathbf{C}, \boldsymbol{\varphi})]_j\, \mathrm{d}V,\\
&K_{\text{f}ij}(\mathbf{C}) = \int_{\Omega_1} (\nabla N_i)^{\text{T}} \nabla N_j \sigma_{\text{r}}(\mathbf{C})\, \mathrm{d}V, \quad M_{ij} = \int_{\Omega_1} N_i N_j\, \mathrm{d}V.
\end{aligned} \tag{48}$$

Here, i and j denote the node numbers.

Moreover, by using Eq. (47), the constraint conditions (38) and (43) can be reformulated into nonlinear algebraic forms. In this way, the phase field problem is transformed into solving a system of nonlinear equations based on the discretized finite elements.

5. Examples and discussions

5.1. Computation model

For illustration, the phase field method described above is employed to simulate the morphological evolution of an initially spherical vesicle placed in the center of the space between two parallel and penny-shaped disk electrodes, as shown in Fig. 2. For such an axisymmetrical problem, the differential and integral operators in the cylindrical coordinate system are expressed as

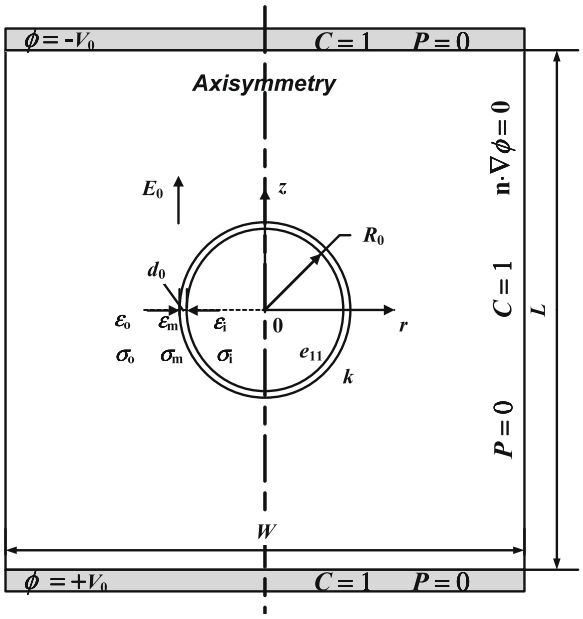

Fig. 2. An axisymmetric vesicle–electrolyte–electrode system subjected to an approximately uniform electric field.

$$\begin{aligned}
&\nabla f = \frac{\partial f}{\partial r}\mathbf{n}_r + \frac{\partial f}{\partial z}\mathbf{n}_z,\\
&|\nabla f|^2 = \left(\frac{\partial f}{\partial r}\right)^2 + \left(\frac{\partial f}{\partial z}\right)^2,\\
&\nabla^2 f = \frac{\partial^2 f}{\partial r^2} + \frac{\partial^2 f}{\partial z^2} + \frac{1}{r}\frac{\partial f}{\partial r},\\
&\int_\Omega g(\mathbf{x})\,\mathrm{d}V = 2\pi\int\int g(r,z) r\,\mathrm{d}r\,\mathrm{d}z,
\end{aligned} \tag{49}$$

where f is an arbitrary function, $g(\mathbf{x})$ is an arbitrary integrand, the coordinate z is along the axisymmetric axis, and r is the radial coordinate.

In our simulations, the initial radius and the membrane thickness of the vesicle are taken to be $R_0 = 10$ μm and $d_0 = 5$ nm, respectively. In order to rule out the boundary effects, we set the diameter and distance of the two circular electrodes as $W = L = 6R_0 = 60$ μm. Specify a positive electric potential $\phi = \phi_0 > 0$ on the bottom electrode and $\phi = -\phi_0$ on the top. In this case, the vesicle is exposed to an approximately uniform electric field $E_0 = 2\phi_0/L$. The insulation condition $\mathbf{n}\cdot\nabla\phi = 0$ is assumed on the side boundary of the axisymmetric model. By virtue of the axisymmetry of the problem, only half of the axial section plane of the model is calculated. The initial condition of the electric potential is $\phi_0 = 0$ at $t = 0$. The Dirichlet boundary condition $C = 1$ and $P = 0$ are used throughout the boundary of the model. The initial conditions of the phase field C and P are taken as

$$\begin{aligned}
C_0 &= \tanh\left(\frac{\sqrt{r^2+z^2} - R_0}{\sqrt{2}b}\right),\\
P_0 &= \frac{3k}{4\sqrt{r^2+z^2}}\left[\tanh\left(\frac{\sqrt{r^2+z^2} - R_0}{\sqrt{2}b}\right) - 1\right](\sqrt{r^2+z^2}c_0 - 2).
\end{aligned} \tag{50}$$

Both the inside and outside of the vesicle are filled with electrolytes, with the dielectric constants ε_i and ε_o, and the conductivities σ_i and σ_o, respectively. The bending stiffness, spontaneous curvature, dielectric constant, conductivity and flexoelectric coefficient of the vesicle membrane are denoted by $k, c_0, \varepsilon_m, \sigma_m$ and e_{11}, respectively. The material parameters used in our calculations are listed in Table 1, in which the values in the *Cell* column were experimentally measured from cells by Kotnik and Miklavcic [58] and Gowrishankar et al. [59], while those in the *Vesicle* column were measured from vesicles by Riske and Dimova [16].

The axisymmetric space is divided into axisymmetric rectangular quadratic Lagrange elements [57] of size 0.75 μm × 0.75 μm, each of which has four Gauss integration points. We take an optimal value of $b = 0.5$ μm in Eq. (50), ensuring that the width of the numerical interface can cover at least one space step. We also compare the results for several different widths. It is found that if a too small width is chosen (e.g., $b = 0.2$ μm), some certain places in the interface would

Table 1
Parameters used in the calculation.

Definitions of parameters	*Cell*	*Vesicle*
Cell (or vesicle) radius, R	1×10^{-5} m	1.76×10^{-5} m
Membrane thickness, d_0	5×10^{-9} m	5×10^{-9} m
Bending stiffness, k	1×10^{-19} J	8×10^{-19} J
Flexoelectric coefficient, e_{11}	1×10^{-10} C/m	0
Conductivity of extracellular medium, σ_o	$1.2\,\mathrm{Sm}^{-1}$	1.2×10^{-2} Sm^{-1}
Conductivity of intracellular medium, σ_i	0.3 Sm^{-1}	6×10^{-4} Sm^{-1}
Conductivity of cell membrane, σ_m	3×10^{-7} Sm^{-1}	3×10^{-7} Sm^{-1}
Dielectric constant intracellular medium, ε_i	6.4×10^{-10} As/Vm	8×10^{-11} As/Vm
Dielectric constant of extracellular medium, ε_o	6.4×10^{-10} As/Vm	8×10^{-11} As/Vm
Dielectric constant of cell membrane, ε_m	4.4×10^{-11} As/Vm	5.5×10^{-12} As/Vm
Spontaneous curvature, c_0	-2.4×10^{5} m^{-1}	-1.36×10^{5} m^{-1}
Diameter, W	6×10^{-5} m	1.56×10^{-4} m
Height, L	6×10^{-5} m	1.56×10^{-4} m

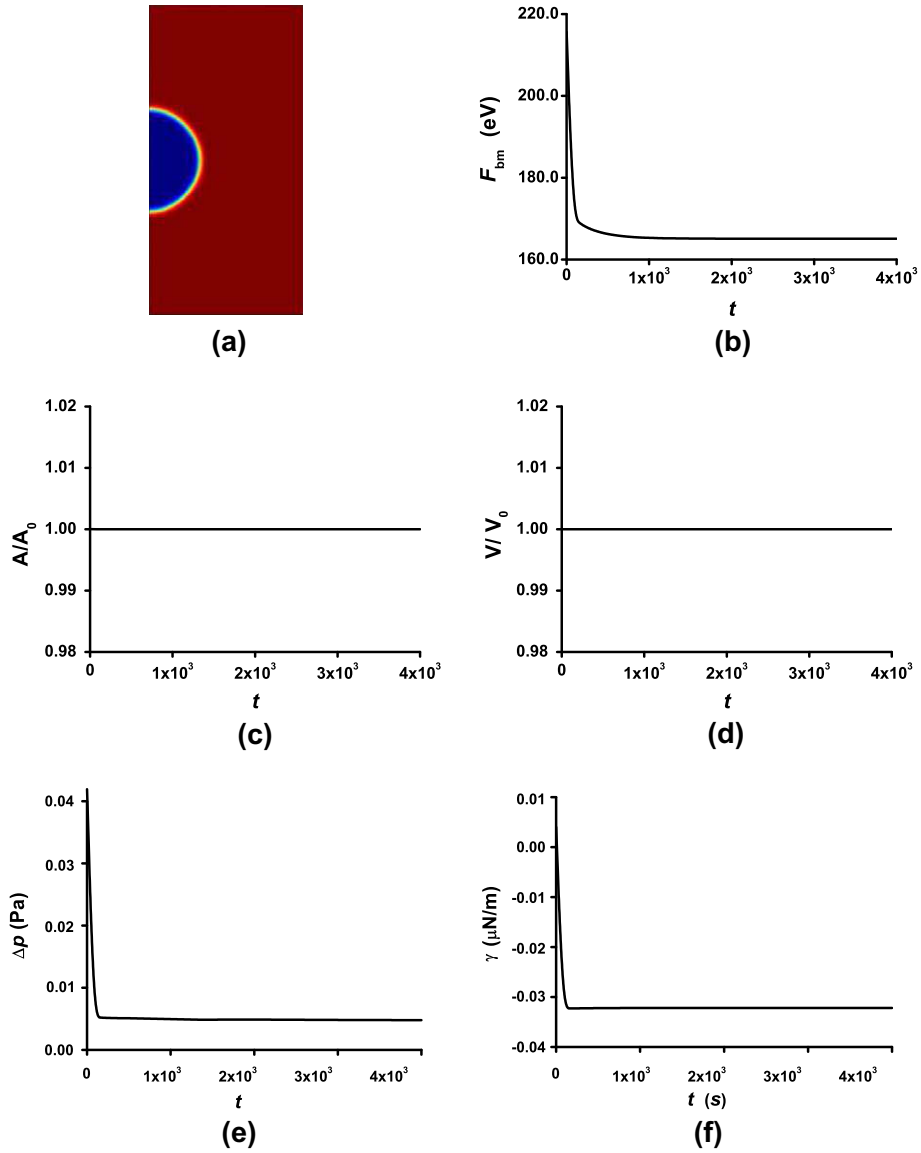

Fig. 3. Simulation results of an initially spherical vesicle in the absence of an electric field ($E_0 = 0$) where the parameters given in the *Cell* column of Table 1 are used.

become fuzzy during the deformation of the vesicle; and if one specifies a too large width (e.g., $b = 2.0$ μm), the original thin interfacial property of vesicle membrane cannot be externalized. The total number of finite elements is 3200. The discrete ordinary differential equation system (47), in conjunction with the volume and area constraint conditions (38) and (43), are solved using the DASPK solver [60], based on the variable-order variable-stepsize backward differentiation method (BDF). Additionally, a self-adapting iteration step strategy is utilized in the time-step determination in order to improve the calculation efficiency. Firstly, an initial time step Δt is specified. Then the values for the variables C and ϕ are calculated at the steps Δt and $0.8\Delta t$, respectively. If the maximum relative error for C and ϕ, $err = \max(\phi_{\mathrm{err}}, C_{\mathrm{err}})$, are within 0.1%, Δt is taken for the calculation of the next step. Otherwise, the step is decreased to $0.8\Delta t$, and the above procedure is repeated until the requirement of the accuracy is satisfied. If the relative error is less than 0.05%, the step will be replaced by $1.2\Delta t$. From our numerical calculation experience, the step Δt may be specified in the range from 0.1 to 100, if the initial step is taken as 40. This adaptive time advancing algorithm ensures the balance of high accuracy and efficiency of the calculation.

5.2. Verification of the calculation algorithm

In the adopted steepest decent approach [55], if the mechanical and electrical energies as well as the osmotic pressure and surface tension converge to constant values, the simulation is stable and the vesicle system is considered to have reached an equilibrium configuration. In order to verify the convergence and stability of the present numerical algorithm,

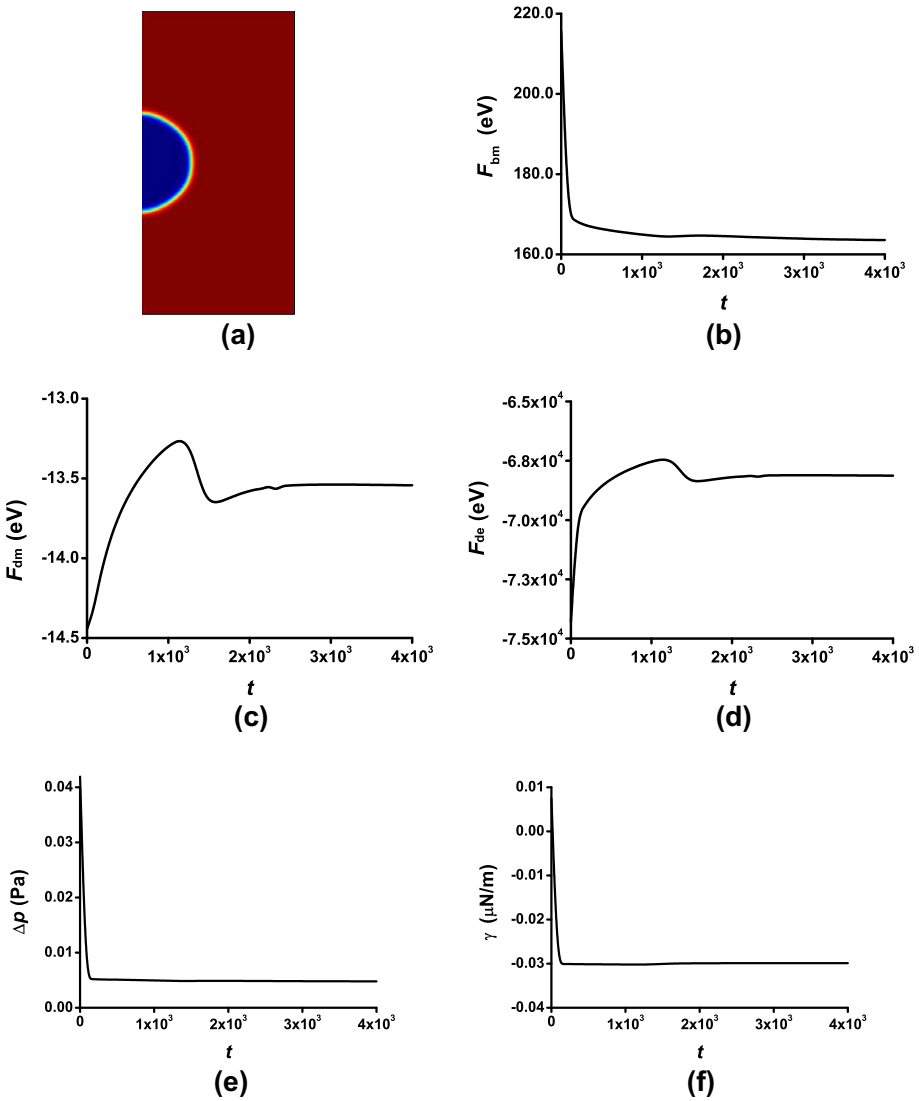

Fig. 4. Simulation results of an initially spherical vesicle under an electric field ($E_0 = 10.0$ kV/m) where no flexoelectric effect has been included, i.e., ($e_{11} = 0$) and the parameters are given in the *Cell* column of Table 1.

we consider three validation cases under conditions: (I) $E_0 = 0$ and $e_{11} = 0$; (II) $E_0 = 10.0\,\mathrm{kV/m}$ and $e_{11} = 0$; (III) $E_0 = 10.0\,\mathrm{kV/m}$ and $e_{11} = 1 \times 10^{-10}\,\mathrm{C/m}$, respectively. The data in the *Cell* column of Table 1 are adopted for the other parameters.

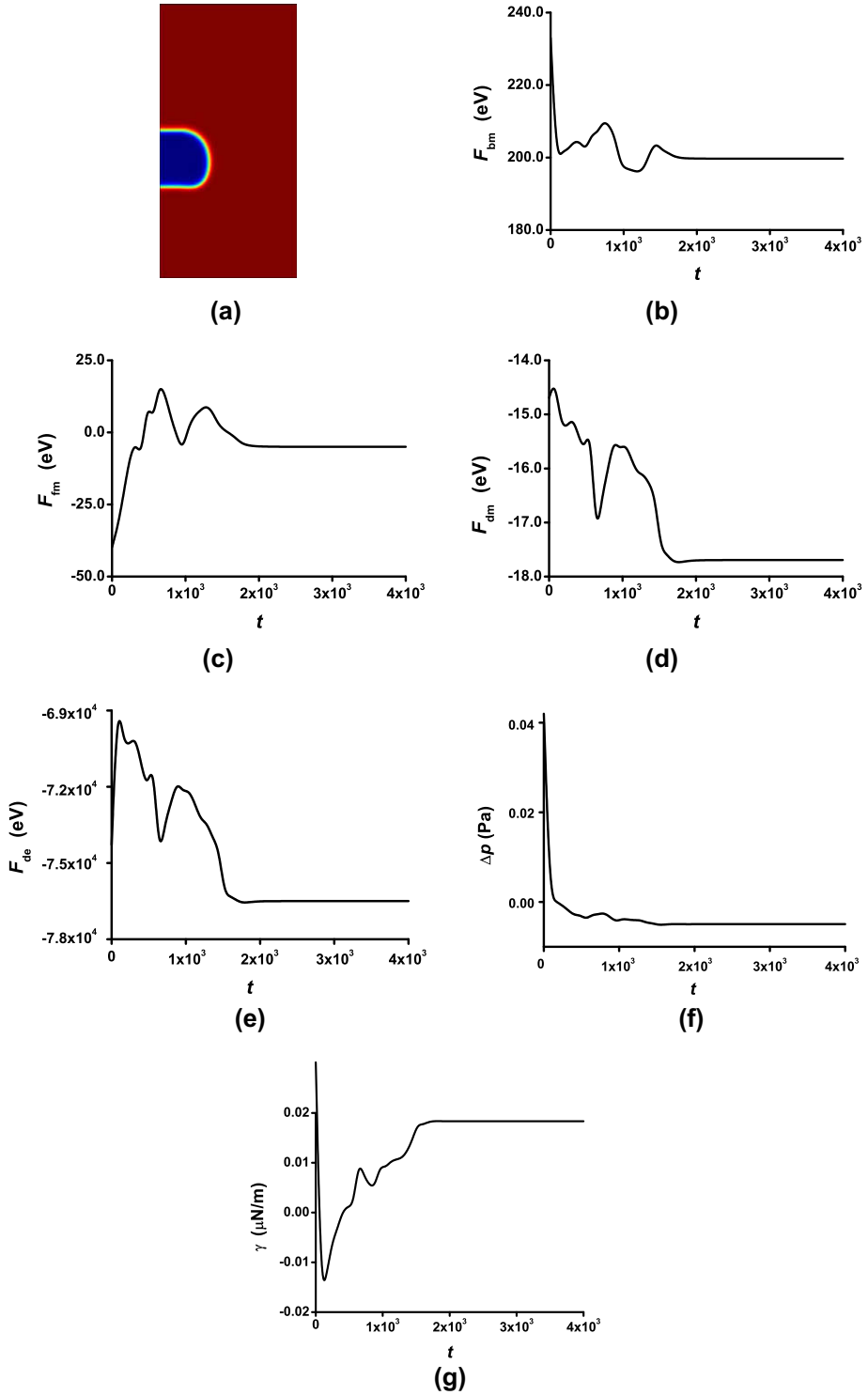

Fig. 5. Simulation results of an initially spherical vesicle under an electric field ($E_0 = 10.0\,\mathrm{V/m}$) with flexoelectric effect ($e_{11} = 1.0 \times 10^{-10}\,\mathrm{C/m}$), where we use the parameters given in the *Cell* column of Table 1.

The calculation results in Case I (without electric effect) are presented in Fig. 3. Fig. 3(a) shows the equilibrium morphology of the vesicle at the iteration step $t = 4000$. The bending energy F_{bm} plotted in Fig. 3(b) decreases from 216 eV at $t = 0$ to a constant value 165 eV at $t = 4000$. Fig. 3(c) and (d) verify that the area and volume are almost kept constant during deformation. The osmotic pressure Δp and the surface tension γ converge to 0.0057 Pa and -0.032 μN/m, respectively (Fig. 3(e) and (f)). When we take the special values $R = 1.0 \times 10^{-5}$ m, $k = 1.0 \times 10^{-19}$ J, and $c_0 = -2.4 \times 10^5$ m^{-1}, as given in Table 1, the following relation is approximately fulfilled:

$$\Delta p + \frac{2\gamma}{R} + \frac{kc_0^2}{R} - \frac{2kc_0}{R^2} = 0, \tag{51}$$

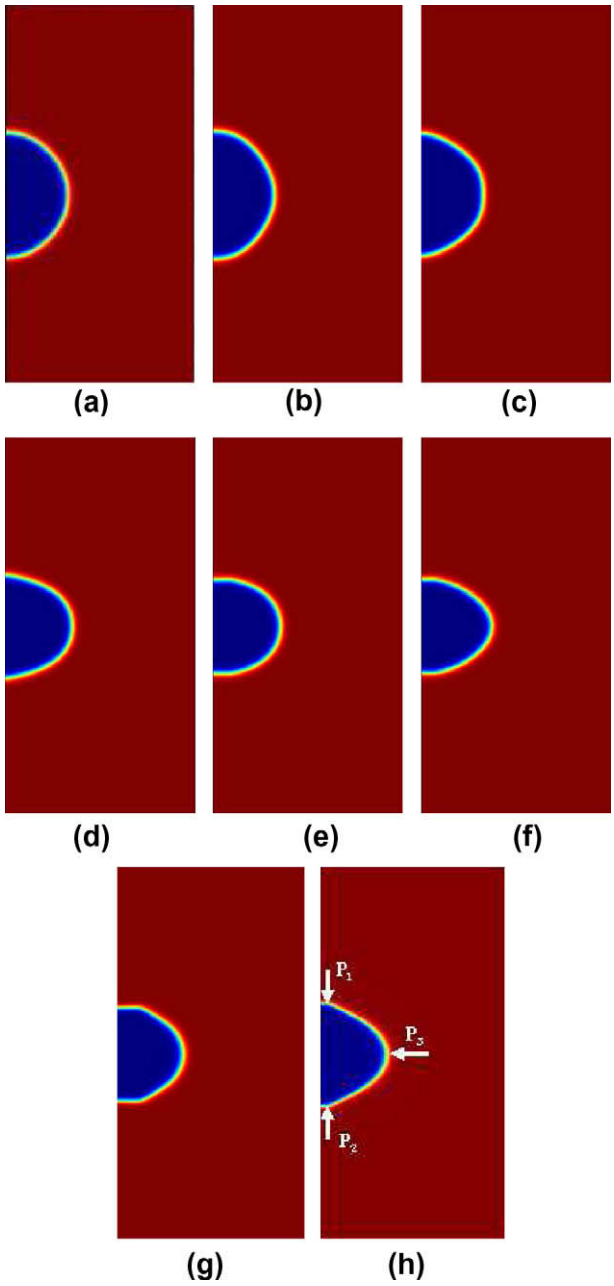

Fig. 6. Shape evolution of a vesicle under an increasing electric field E_0 (from 0 to 70.0 kV/m) where no flexoelectric effect has been included ($e_{11} = 0$). Here we take the conductivity coefficients $\sigma_i = 0.3$ Sm^{-1} and $\sigma_o = 1.2$ Sm^{-1}, and the other parameters are given in the *Cell* column of Table 1. In the blue and the red regions, we have $C = -1$ and $C = 1$, respectively. (For interpretation of the references to colour in this figure legend, the reader is referred to the web version of this article.)

which is consistent with the theoretical prediction of the stable shape for a spherical configuration by Ou-Yang et al. [21].

In Case II, where an electric field is applied but the effect of flexoelectricity is neglected, the calculation results (Fig. 4) are very similar to those in Fig. 3. Fig. 4(c) and Fig. 5(d) show that the dielectric energy of the vesicle and the dielectric energy of the electrolytes converge to $F_{dm} = -13.54$ eV and $F_{de} = -6.8 \times 10^4$ eV, respectively.

Fig. 5 plots the simulation results in Case III, where the effect of flexoelectricity has been taken into account. The vesicle shape in this case (Fig. 5(a)) is significantly different from those in Fig. 3(a) and Fig. 4(a). The vesicle evolves from the initial spherical shape to a drum-like shape. The lower surface of the final configuration is larger and flatter than the upper surface. It is also found that the vesicle shifts downwards by a short distance. The flexoelectric energy (Fig. 5(c)) induced by the applied electric loading approaches $F_{fm} = -4.98$ eV, only about 2.5% of the bending energy (Fig. 5(b)). This example demonstrates that, although the flexoelectric energy constitutes only a small portion of the total energy, it can nevertheless play a significant role in the morphological transition of cells and vesicles. Moreover, the dielectric energy of the membrane

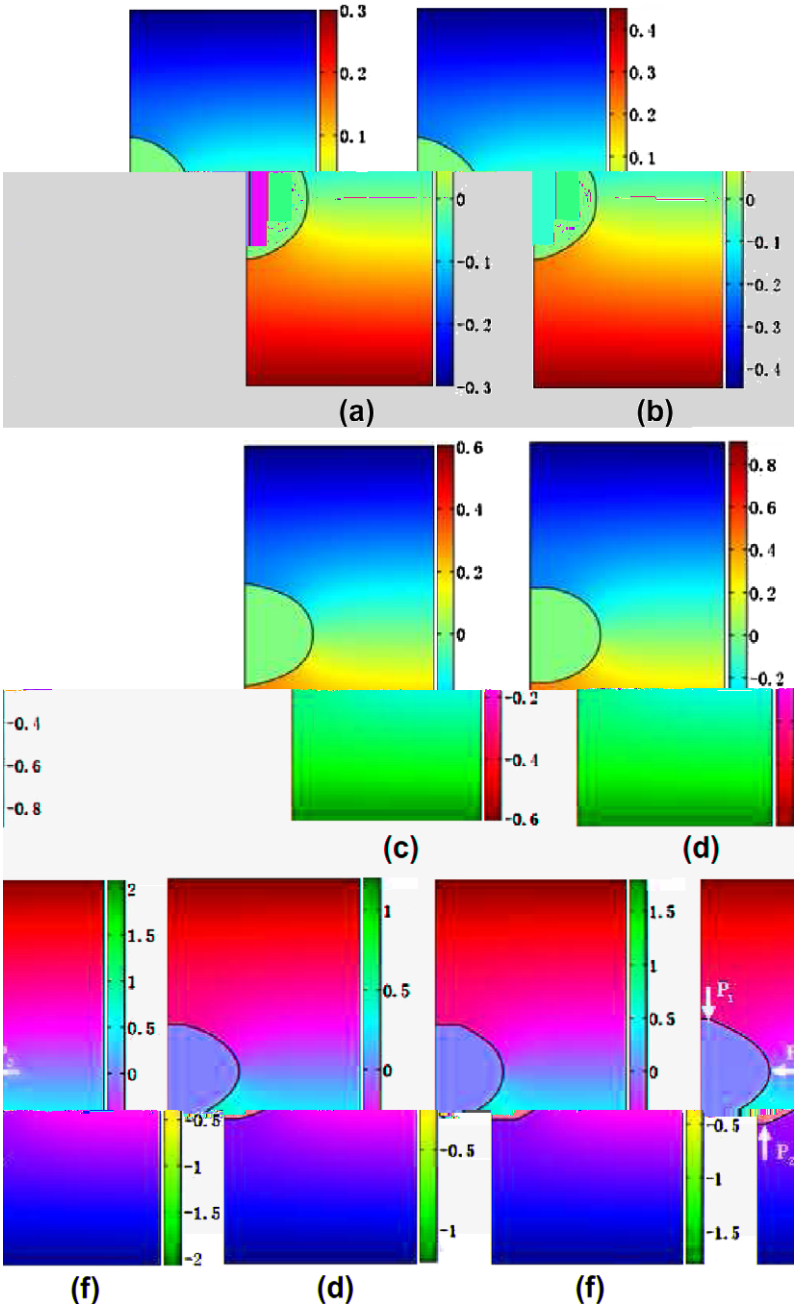

Fig. 7. Variation of the electric potential field ϕ corresponding to the morphological evolution in Fig. 6 under an increasing electric field E_0 from 0 to 70.0 kV/m, where we take $e_{11} = 0, \sigma_i = 0.3\ \mathrm{Sm}^{-1}$, and $\sigma_o = 1.2\ \mathrm{Sm}^{-1}$.

(Fig. 5(d)), the osmotic pressure (Fig. 5(f)), and the surface tension (Fig. 5(g)) in the stable configuration of Case III are dramatically different from those in Cases I and II, but the dielectric energy (Fig. 5(e)) seems to make little difference in the morphology of the vesicle.

We have compared the calculation results under three different finite element meshes with element numbers $60 \times 100, 50 \times 90$, and 80×160, respectively. The corresponding solutions are in good agreement, demonstrating the size insensitivity and the robustness of the present algorithm.

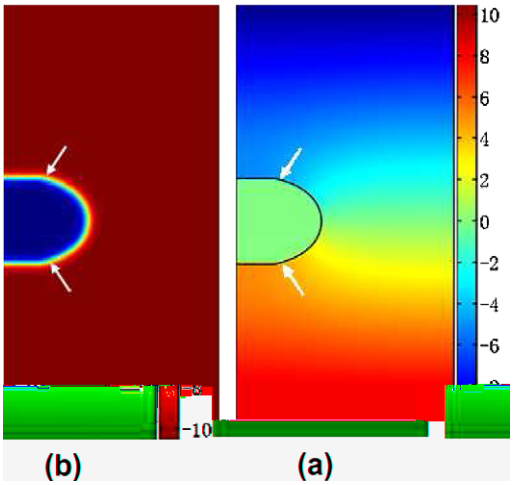

Fig. 8. Simulation results based on the experimentally measured parameters for a vesicle under an externally applied electric field [16], which are given in the *Vesicle* column of Table 1.

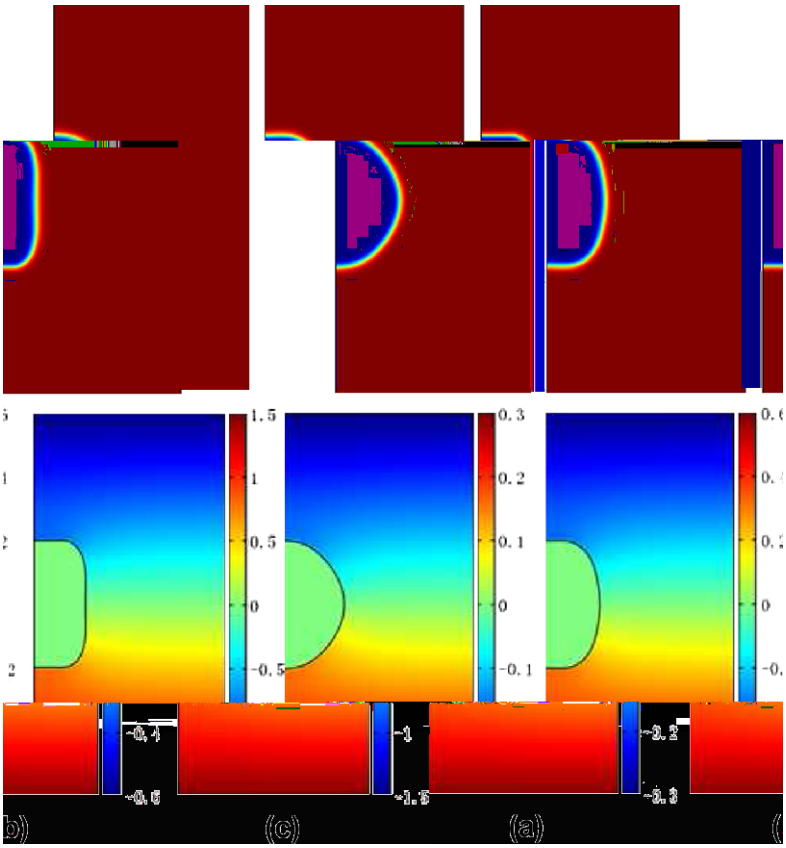

Fig. 9. Shape evolution and the corresponding electric potential field E_0 from 10.0 to 50.0 kV/m, where the effect of flexoelectricity has been neglected (i.e., $e_{11} = 0$). The other parameters adopted are given in the *Cell* column of Table 1.

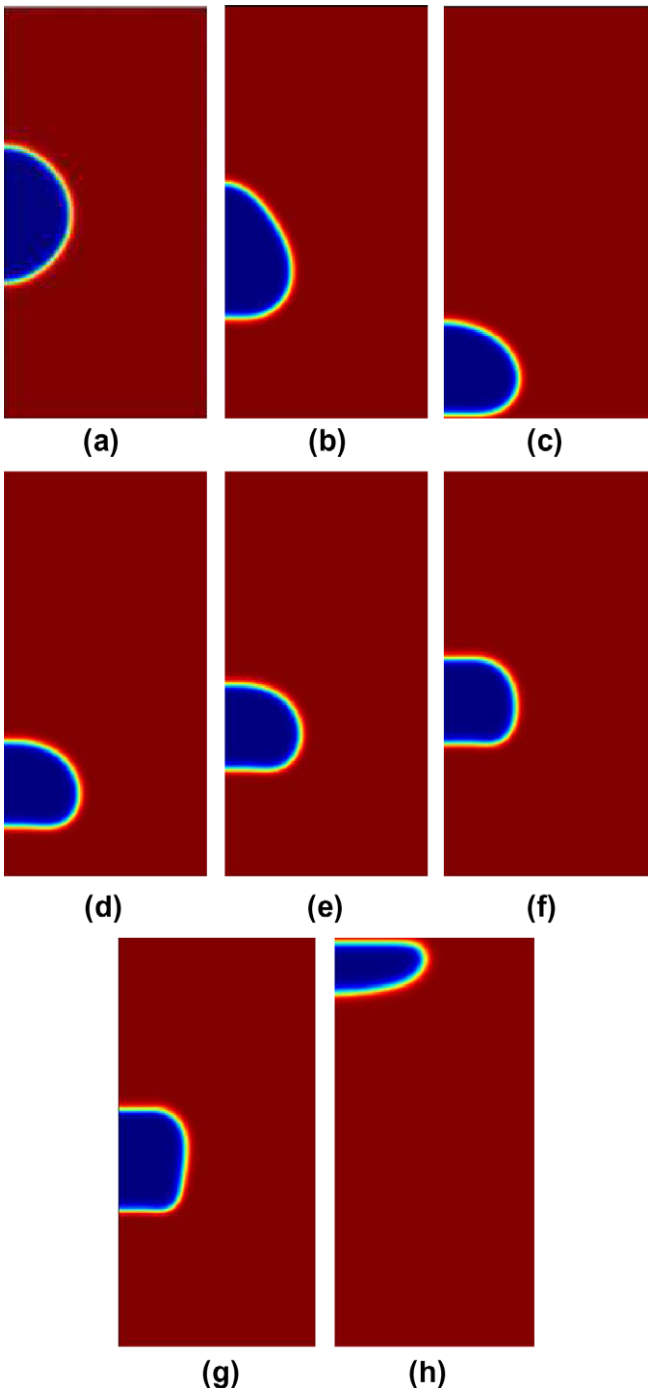

Fig. 10. Shape evolution of a vesicle under an increasing electric field E_0 from 0 to 14.0 kV/m, where we take the effect of flexoelectric coefficient $e_{11} = 1.0 \times 10^{-10}$ C/m. The other parameters are given in the *Cell* column of Table 1. The blue and the red regions have $C = -1$ and $C = 1$, respectively. (For interpretation of the references to colour in this figure legend, the reader is referred to the web version of this article.)

5.3. Morphological evolution of vesicles under electric fields

In what follows, we will simulate the morphological evolution of a vesicle under an increasing electric field E_0 and examine the influences of such key parameters as the flexoelectric coefficient e_{11} of the membrane and the conductivity coefficients σ_o and σ_i of the outer and inner electrolytes. The data in the *Cell* column of Table 1 are used in our simulations, except where otherwise stated.

The evolutions of the phase field C and the electric potential field ϕ under an increasing electric field are shown in Figs. 6 and 7, where the conductivity coefficient of the outer electrolyte is taken to be larger than that of the inner and the membrane flexoelectricity is neglected (i.e., $\sigma_o > \sigma_i$ and $e_{11} = 0$). As E_0 rises from 0 to 40 kV/m, the initially spherical vesicle becomes oblate, as shown in Fig. 6(a)–(f). Such a shape change is in agreement with the theoretical prediction of Hyuga et al. [32]. With further increase in E_0, the top and bottom parts of the membrane gradually flatten, rendering the vesicle into a drum shape (Fig. 6(g) and Fig. 7(h)). This interesting transformation was recently observed in experiments by Riske and Dimova [16] but has not been elucidated theoretically. When E_0 reaches 70.0 kV/m, the phase field gap becomes nonhomogeneous, indicating a nonuniform variation of the thickness of the vesicle. At points P_1 and P_2, the vesicle becomes thinner and thinner due to strain concentration, while at point P_3, the thickness increases gradually, as shown in Fig. 6(h) and Fig. 7(g). Therefore, a sufficiently high electric field may induce electroporation or rupture in the vesicle at positions P_1 and P_2.

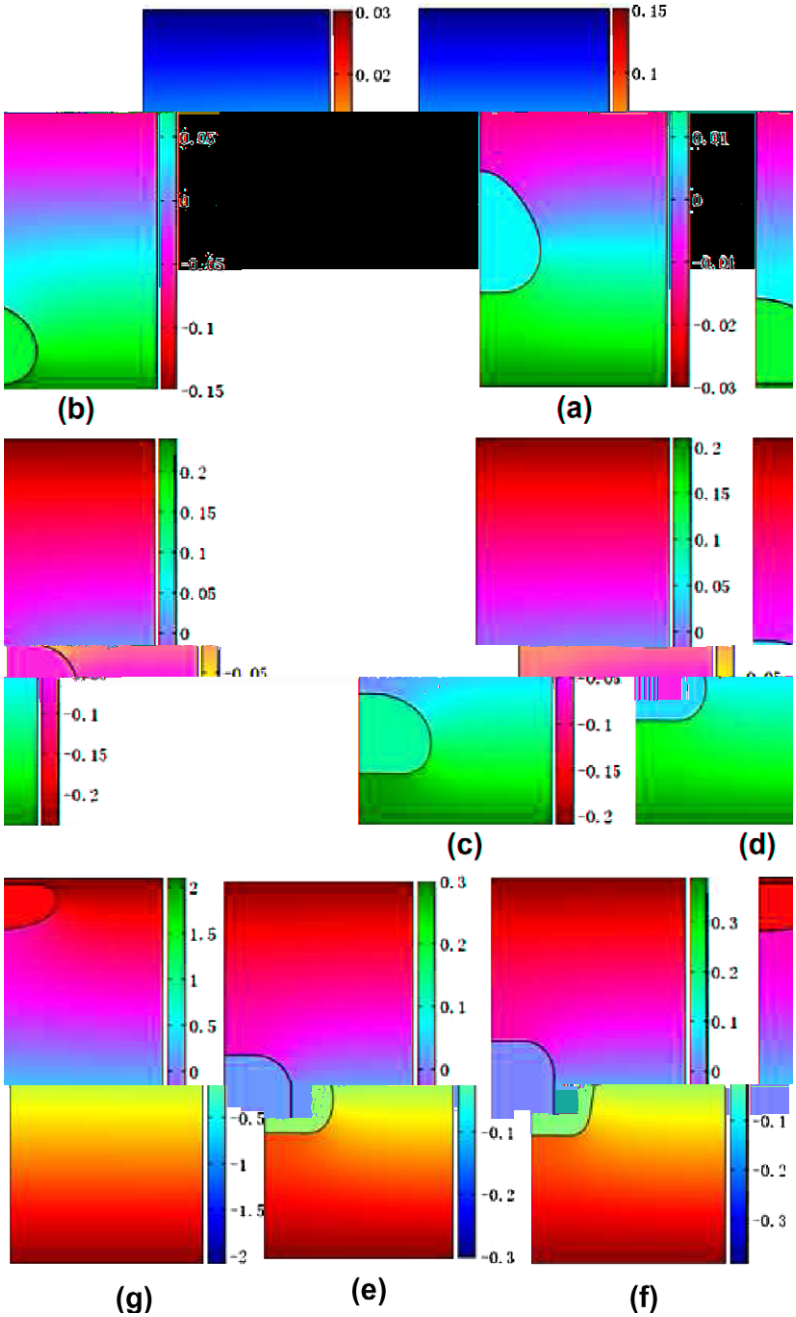

Fig. 11. Variation of the electric potential field ϕ corresponding to the morphological evolution in Fig. 10 under an increasing electric field E_0.

To further verify the sphere-to-drum shape transition shown in Fig. 6(a)–(g), we repeated the simulation using the parameter values measured experimentally from vesicles under an electric field by Riske and Dimova [16], which are listed in the *Vesicle* column of Table 1. The externally applied electric field E_0 changes from 0 to 200 kV/m. The obtained results for the phase field and the electric potential field are displayed in Fig. 8. Again, we observed the transition of the vesicle from a sphere shape to a drum, in consistency with the recent experimental results of Riske and Dimova [16].

As experimentally observed by Riske and Dimova [16], the drum-like shape configuration is unstable and short-lived under a high electric field. Our previous study [19] showed that the electric field can become singular at some particular positions. The instability of this shape might be attributed to such reasons as electroporation associated with the singularity of the electrical field and the associated localization of deformation at these positions. During electroporation, the volume and surface area of the vesicle may change due to mass transport, and the vesicle eventually reverts back to an oblate shape in the electric field. The detailed considerations about the electroporation and the post-instability evolution are beyond the scope of the present study.

5.4. Effects of the conductivities of the inner and outer electrolytes

The conductivity σ_m of the vesicle is usually much smaller than those of the electrolytes, which we have taken to be $\sigma_i = 0.3\ \mathrm{Sm}^{-1}$ and $\sigma_i = 1.2\ \mathrm{Sm}^{-1}$ in Fig. 2. To further examine the effects of the conductivity of the inner and outer electrolytes, we exchange the values of their conductivity coefficients, that is, $\sigma_i = 1.2\ \mathrm{Sm}^{-1}$ and $\sigma_i = 0.3\ \mathrm{Sm}^{-1}$. Fig. 9 shows the corresponding results of the phase field and the electric potential under an increasing electric field E_0. It is seen from Fig. 9(a) and (b) that the vesicle deforms from a sphere to a prolate as E_0 rises from 10.0 kV/m to 20.0 kV/m, in consistency with the theoretical prediction of Hyuga et al. [32] under the same condition. When the electric field E_0 increases to $E_0 = 50.0$ kV/m, a long cylinder-like vesicle morphology is obtained (Fig. 9(c)). This solution is in accord with the experimental observations of Riske and Dimova [16]. Therefore, it may be concluded that the conductive properties of the inner and outer electrolytes play a crucial role in the morphology evolution of vesicles under electric loading.

5.5. Effects of flexoelectricity

As already mentioned above, the flexoelectric effect can have a significant influence on the morphology of vesicles. To further explore this issue, we simulate the morphological evolution of a vesicle with a flexoelectric coefficient of

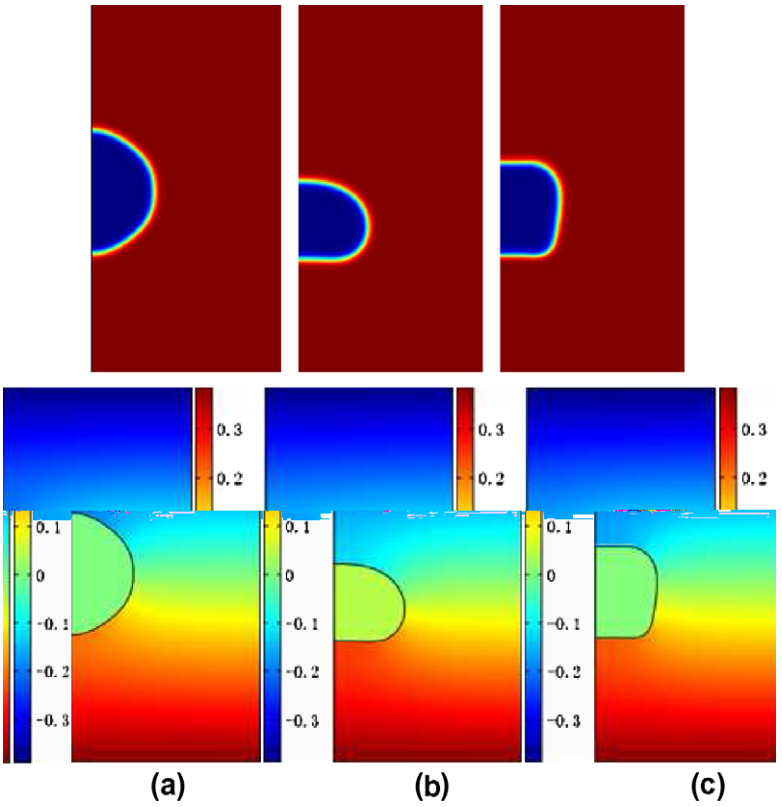

Fig. 12. Comparison of the stable morphological evolution and the corresponding electric potential of a vesicle under three representative flexoelectric coefficients: (a) $e_{11} = 0$, (b) $e_{11} = 2.5 \times 10^{-11}$ C/m, (c) $e_{11} = 1.0 \times 10^{-10}$ C/m and electric field $E_0 = 13.0$ kV/m.

$e_{11} = 1.0 \times 10^{-10}$ C/m. The corresponding distributions of the phase field and the electric field are shown in Figs. 10 and 11 under several representative values of the applied electric field E_0. It is seen that all stable shapes of the vesicle under different values of E_0 are asymmetric in the direction of the electric field. As E_0 rises in the range of 0—5.0 kV/m, the bottom part of the vesicle gradually flattens and the deformed vesicle moves downward to a new equilibrium position (Fig. 10(a)–(c) or Fig. 11(a)–(b)). For $E_0 = 5.0$ kV/m, the equilibrium position of the vesicle, which has a semi-ellipsoidal shape, is near the bottom of the simulation box.

In the range of $5.0 \text{ kV/m} < E_0 \leqslant 14.0$ kV/m, the top part of the vesicle also becomes flatter and flatter, displaying an interesting transition from a semi-ellipsoid to a drum and, finally, to an oblate. The corresponding equilibrium position moves upward to the top of the simulation box (Fig. 10(c)–(h) or Fig. 11(b)–(g)).

We also compare the results for three representative flexoelectric coefficients, $e_{11} = 0, e_{11} = 2.5 \times 10^{-11}$ C/m, and $e_{11} = 1 \times 10^{-10}$ C/m, as shown in Fig. 12. Evidently, the stable morphology of a vesicle is sensitive to its flexoelectric coefficient. These results show that the flexoelectric effect can not only induce significant variations and asymmetry in the morphology of vesicles, but can also change the equilibrium position of the vesicle in the electric field. This suggests possible utilization of the flexoelectric effects in manipulating and controlling of cells or vesicles.

6. Conclusions

Based on a coupled mechanical–electrical liquid crystal model, we have developed a finite element-based phase field method to investigate the morphological evolution of a vesicle in an electric field. The influences of such factors as elastic bending, flexoelectricity, and dielectricity have been taken into account. The vesicle shape equation and the electric field equation are formulated in terms of the phase field function and the electric potential. After discretization, these equations are solved by the finite element method. To demonstrate the validity and efficiency of this approach, we have considered the evolution of an initially spherical vesicle under an increasing electric field. The obtained results are consistent with previous theoretical predictions for several special configurations by Ou-Yang et al. [21] and Hyuga et al. [32] as well as recent experimental observations by Riske and Dimova [16]. We showed that the applied electric field leads to an interesting shape transition of vesicles and that the membrane flexoelectricity can play a dominant role in this process. This finite element based phase field method can efficiently handle the strong nonlinearity and large deformation in the present problem. The simulation results indicate that the flexoelectric effects could potentially be used in manipulation of cells and vesicles and controlling their morphology and migration.

Acknowledgments

Supports from the National Natural Science Foundation of China (Grant Nos. 10525210, 10732050, and 10802041) and the 973 Program of MOST (Grant No. 2004CB619300) are gratefully acknowledged. The first author also acknowledges the financial support from China Postdoctoral Science Foundation.

References

[1] R. Lipowsky, E. Sackmann, Structure and Dynamics of Membranes, Elsevier, Amsterdam, 1995.
[2] Y. Yawata, Cell Membrane: The Red Blood Cell as a Model, Wiley-VCH, Weinheim, 2003.
[3] C.D. McCaig, A.M. Rajnicek, B. Song, M. Zhao, Controlling cell behavior electrically: current views and future potential, Physiol. Rev. 85 (3) (2005) 943–978.
[4] J. Voldman, Electrical forces for microscale cell manipulation, Annu. Rev. Biomed. Eng. 8 (1) (2006) 425–454.
[5] E. Neumann, Electroporation and Electrofusion in Cell Biology, Springer-Verlag, New York, 1989.
[6] B.M. Chassy, Guide to Electroporation and Electrofusion, Academic Press, New York, 1991.
[7] J.C. Weaver, Electroporation: a general phenomenon for manipulating cells and tissue, J. Cell Biochem. 51 (1993) 426–435.
[8] G. Cevc, H. Richardsen, Lipid vesicles and membrane fusion, Adv. Drug Deliver. Rev. 38 (3) (1999) 207–232.
[9] A.G. Petrov, The Lyotropic States of Matter: Molecular Physics and Living Matter Physics, Gordon & Breach Publishers, New York, 1999.
[10] J.N. Mehrishi, J. Bauer, Electrophoresis of cells and the biological relevance of surface charge, Electrophoresis 23 (13) (2002) 1984–1994.
[11] J.C. Weaver, Electroporation of biological membranes from multicellular to nano scales, IEEE Trans. Dielect. Elect. Insul. 10 (5) (2003) 754–768.
[12] C. Chen, S.W. Smye, M.P. Robinson, J.A. Evans, Membrane electroporation theories: a review, Med. Biol. Eng. Comput. 44 (1–2) (2006) 5–14.
[13] K.A. Riske, R. Dimova, Electro-deformation and poration of giant vesicles viewed with high temporal resolution, Biophys. J. 88 (2005) 1143–1155.
[14] K.A. Riske, R. Dimova, Timescales involved in electro-deformation, poration and fusion of giant vesicles resolved with fast digital imaging, Biophys. J. 88 (2005) 241.
[15] C.K. Haluska, K.A. Riske, V. Marchi-Artzner, J.M. Lehn, R. Lipowsky, R. Dimova, From the cover: time scales of membrane fusion revealed by direct imaging of vesicle fusion with high temporal resolution, PNAS 103 (2006) 15841–15846.
[16] K.A. Riske, R. Dimova, Electric pulses induce cylindrical deformations on giant vesicles in salt solutions, Biophys. J. 91 (5) (2006) 1778–1786.
[17] R. Dimova, S. Aranda, N. Bezlyepkina, V. Nikolov, K.A. Riske, R. Lipowsky, A practical guide to giant vesicles. Probing the membrane nanoregime via optical microscopy, J. Phys.: Condens. Matter. 18 (2006) S1151–S1176.
[18] R. Dimova, K.A. Riske, S. Aranda, N. Bezlyepkina, R.L. Knorr, R. Lipowsky, Review: giant vesicles in electric fields, Soft Matter 3 (2007) 817–927.
[19] L.T. Gao, X.Q. Feng, Y.J. Yin, H.J. Gao, A liquid crystal model of vesicles under mechanical and electric fields, J. Mech. Phys. Solids 56 (2008) 2844–2862.
[20] U. Seifert, Configurations of fluid membranes and vesicles, Adv. Phys. 46 (1) (1997) 13–137.
[21] Z.C. Ou-Yang, J.X. Liu, Y.Z. Xie, Geometric Methods in the Elastic Theory of Membranes in Liquid Crystal Phases, World Scientific, Singapore, 1999.
[22] M. Kraus, W. Wintz, U. Seifert, R. Lipowsky, Fluid vesicles in shear flow, Phys. Rev. Lett. 77 (1996) 3685.
[23] U. Seifert, Fluid membranes in hydrodynamic flow fields: formalism and an application to fluctuating quasispherical vesicles in shear flow, Eur. Phys. J. B 8 (1999) 405.

[24] H. Noguchi, G. Gompper, Dynamics of fluid vesicles in shear flow: effect of membrane viscosity and thermal fluctuations, Phys. Rev. E 72 (2005) 011901.
[25] I. Cantat, C. Misbah, Dynamics and similarity laws for adhering vesicles in haptotaxis, Phys. Rev. Lett. 83 (1999) 235.
[26] I. Cantat, C. Misbah, Lift force and dynamical unbinding of adhering vesicles under shear flow, Phys. Rev. Lett. 83 (1999) 880.
[27] C. Misbah, Vacillating breathing and tumbling of vesicles under shear flow, Phys. Rev. Lett. 96 (2006) 028104.
[28] H. Noguchi, G. Gompper, Swinging and tumbling of fluid vesicles in shear flow, Phys. Rev. Lett. 98 (2007) 128103.
[29] K. Brakke, The surface evolver, Exp. Math. 1 (2) (1992) 141–165.
[30] F. Feng, W.S. Klug, Finite element modeling of lipid bilayer membranes, J. Comput. Phys. 220 (2006) 394–408.
[31] L. Ma, W.S. Klug, Viscous regularization and r-adaptive remeshing for finite element analysis of lipid membrane mechanics, J. Comput. Phys. 227 (2008) 5816–5835.
[32] H. Hyuga, K. Kinosita Jr., N. Wakabayashi, Deformation of vesicles under the influence of strong electric fields, Jap. J. Appl. Phys. 30 (5) (1991) 1141–1148.
[33] H. Hyuga, K. Kinosita Jr., N. Wakabayashi, Deformation of vesicles under the influence of strong electric fields II, Jap. J. Appl. Phys. 30 (6) (1991) 1333–1335.
[34] T.H. Fan, A.G. Fedorov, Electrohydrodynamics and surface force analysis in AFM imaging of a deformable charged, biological membrane in a dilute electrolyte solution, Langmuir 19 (26) (2003) 10930–10939.
[35] T. Biben, K. Kassner, C. Misbah, Phase-field approach to three-dimensional vesicle dynamics, Phys. Rev. E 72 (2005) 041921.
[36] J.A. Sethian, Level Set Methods and Fast Marching Methods, Cambridge University Press, Cambridge, 1999.
[37] S. Osher, R. Fedkiw, Level Set Methods and Dynamic Implicit Surfaces, Springer-Verlag, 2002.
[38] T. Belytschko, W.K. Liu, B. Moran, Nonlinear Finite Elements for Continua and Structures, John Wiley & Son, New York, 2000.
[39] L.Q. Chen, Phase-field models for microstructure evolution, Annu. Rev. Mater. Res. 32 (2002) 113–140.
[40] T. Biben, C. Misbah, Tumbling of vesicles under shear flow within an advected-field approach, Phys. Rev. E 67 (2003) 031908.
[41] Q. Du, C. Liu, X.Q. Wang, A phase field approach in the numerical study of the elastic bending energy for vesicle membranes, J. Comput. Phys. 198 (2) (2004) 450–468.
[42] F. Campelo, A. Hernandez-Machado, Dynamic model and stationary shapes of fluid vesicles, Eur. Phys. J. E 20 (1) (2006) 37–45.
[43] Q. Du, L.Y. Zhu, Analysis of a mixed finite element method for a phase field bending elasticity model of vesicle membrane deformation, J. Comput. Math. 24 (3) (2006) 265–280.
[44] Q. Du, M. Li, C. Liu, Analysis of a phase field Navier–Stokes vesicle-fluid interaction model, Disc. Cont. Dyn. Sys. B 8 (3) (2007) 539–556.
[45] Q. Du, J. Zhang, Adaptive finite element method for a phase field bending elasticity model of vesicle membrane deformations, SIAM J. Sci. Comput. 30 (3) (2008) 1634–1657.
[46] H.B. Glenn, J.J. Wolken, Liquid Crystals and Biological Structures, Academic Press, New York, 1979.
[47] U. Seifert, Configurations of fluid membranes and vesicles, Adv. Phys. 46 (1997) 13–137.
[48] R. Rosso, M. Verani, E.G. Virga, Second variation of the energy functional for adhering vesicles in two space dimensions, J. Phys. A: Math. Gen. 36 (2003) 12475–12493.
[49] M. Brinkmann, J. Kierfeld, R. Lipowsky, A general stability criterion for droplets on structured substrates, J. Phys. A: Math. Gen. 37 (2004) 11429–11547.
[50] W.D. Shi, X.Q. Feng, H.J. Gao, Two-dimensional model of vesicle adhesion on curved substrates, Acta Mech. Sinica 22 (2006) 529–535.
[51] A.C. Eringen, Microcontinuum Field Theories II: Fluent Media, Springer, New York, 2001.
[52] W. Helfrich, Elastic properties of lipid bilayers: theory and possible experiments, Z. Naturforsch. C 28 (11) (1973) 693–703.
[53] P.G. de Gennes, J. Prost, The Physics of Liquid Crystals (International Series of Monographs on Physics), Oxford University Press, USA, 1994.
[54] X. Wang, Phase Field Models and Simulations of Vesicle Bio-Membranes, Ph.D. Thesis. PQDT, The Pennsylvania State University, USA, 2005.
[55] W.H. Press, B.P. Flannery, S.A. Teukolsky, W.T. Vetterling, Numerical Recipes in C/C++: The Art of Scientific Computing, Cambridge University Press, Cambridge, 2002.
[56] R. Fletcher, Practical Methods of Optimization, John Wiley & Son Ltd., Chichester, 2000.
[57] O.C. Zienkiewicz, R.L. Taylor, The Finite Element Method, The Basis, fifth ed., vol. 1, Butterworth-Heinemann, Oxford, 2000.
[58] T. Kotnik, D. Miklavcic, Second-order model of membrane electric field induced by alternating external electric fields, IEEE Trans. Biomed. Eng. 47 (8) (2000) 1074–1081.
[59] T.R. Gowrishankar, D.A. Stewart, J.C. Weaver, Model of a confined spherical cell in uniform and heterogeneous applied electric fields, Bioelectrochemistry 68 (2) (2006) 181–190.
[60] P.N. Brown, A.C. Hindmarsh, L.R. Petzold, Using Krylov methods in the solution of large-scale differential–algebraic systems, SIAM J. Sci. Comput. 15 (1994) 1467–1488.